Plant Physiology and Biochemistry 136 (2019) 155–161

Contents lists available at ScienceDirect

Plant Physiology and Biochemistry

journal homepage: www.elsevier.com/locate/plaphy

Research article

Molecular insights of a xyloglucan endo-transglycosylase/hydrolase of radiata pine (PrXTH1) expressed in response to inclination: Kinetics and computational study

Luis Morales-Quintana[a,b], Cristian Carrasco-Orellana[a], Dina Beltrán[a], María Alejandra Moya-León[a], Raúl Herrera[a,*]

[a] Functional Genomics, Biochemistry and Plant Physiology, Instituto de Ciencias Biológicas, Universidad de Talca, Campus Lircay s/n, Talca, Chile
[b] Multidisciplinary Agroindustry Research Laboratory, Instituto de Ciencias Biomédicas, Universidad Autónoma de Chile, 5 poniente #1670, Talca, Chile

ARTICLE INFO

Keywords:
Plant cell wall
Xyloglucan endotransglycosylase/hydrolases
Enzymatic parameters
Xyloglycans

ABSTRACT

Xyloglucan endotransglycosylase/hydrolases (XTH) may have endotransglycosylase (XET) and/or hydrolase (XEH) activities. Previous studies confirmed XET activity for PrXTH1 protein from radiata pine. XTHs could interact with many hemicellulose substrates, but the favorite substrate of PrXTH1 is still unknown. The prediction of union type and energy stability of the complexes formed between PrXTH1 and different substrates (XXXGXXXG, XXFGXXFG, XLFGXLFG and cellulose) were determined using bioinformatics tools. Molecular Docking, Molecular Dynamics, MM-GBSA and Electrostatic Potential Calculations were employed to predict the binding modes, free energies of interaction and the distribution of electrostatic charge. The results suggest that the enzyme formed more stable complexes with hemicellulose substrates than cellulose, and the best ligand was the xyloglucan XLFGXLFG (free energy of -58.83 ± 0.8 kcal mol^{-1}). During molecular dynamics trajectories, hemicellulose fibers showed greater stability than cellulose. Additionally, the kinetic properties of PrXTH1 enzyme were determined. The recombinant protein was active and showed an optimal pH 5.0 and optimal temperature of 37 °C. A Km value of 20.9 mM was determined for xyloglucan oligomer. PrXTH1 is able to interact with different xyloglycans structures but no activity was observed for cellulose as substrate, remodeling cell wall structure in response to inclination.

1. Introduction

The loss of vertical growth in trees triggers molecular and biochemical events, which leads morphological changes to restore verticality (Muday, 2001; Ramos and Herrera, 2013). These events involve the perception of gravity and its subsequent transduction into physiological signals inducing differential growth along the stem or affected organ. It promotes cell wall loosening, due to cell wall modifications orchestrated by a battery of enzymes. In pine tree, in order to understand the molecular gravitropic response the enzymes involved in these modifications have been studied[3–6]. Several genes were differentially expressed in inclined radiata pine seedlings depending on time of inclination or the stem side (Ramos et al., 2012, 2016; Valenzuela et al., 2014; Mateluna et al., 2017; Gomez et al., 2018). Among them, PrXTH1 was identified to be highly expressed in the lower side of inclined stems (Valenzuela et al., 2014), suggesting an active participation of this enzyme in cell wall reorganization.

Plant cell walls are a complex supra-molecular assembly that displays diverse structures. Thus, the crystalline cellulose microfibrils are embedded in a matrix of amorphous non-cellulosic polysaccharides such as pectins and hemicelluloses, such as heteroxylans, xyloglucans (XG), (1,3; 1,4)-β-D-glucans, galactomannans/glucomannans, and other polysaccharides, as well as inorganic molecules and proteins (Carpita et al., 2000). In higher plants, the most common XG are polymers of the following repetitive units: XXXG, XXLG, XLXG, XXFG, XLLG and XLFG (Hoffman et al., 2005; Hsieh and Harris, 2009; Peña et al., 2008), where each letter represents a type of substitution at C (O) 6 in the backbone of glucosyl residues, so the α-D-xylopyranosyl residues are indicated with X letter, α-D-xylopyranosyl-β-D-galactopyranosyl are indicated with L letter or α-D-xylopyranosyl-β-D-galactopyranosyl-α-L-fucopyranosyl oligosaccharide are indicated with F letter (Fry et al., 1993; Tuomivaara et al., 2015).

Xyloglucan endotransglycosylase/hydrolase (XTH) enzymes hold transglycosylase (XET), hydrolase (XEH), or both activities (Campbell

* Corresponding author.
E-mail address: raherre@utalca.cl (R. Herrera).

https://doi.org/10.1016/j.plaphy.2019.01.016
Received 12 October 2018; Received in revised form 25 December 2018; Accepted 14 January 2019
Available online 19 January 2019
0981-9428/

Table 1
Purification of recombinant PrXTH1 protein expressed in *P. pastoris*.

Fraction	Volume (mL)	Protein (mg/mL)	XET activity (a.u. μg^{-1} h^{-1})	XEH activity (a.u. μg^{-1} h^{-1})	Purification fold
Concentrated crude extract	10	7.06	2.9 ± 1.1	–	1
Anion exchange chromatography				–	
Eluted protein (0.5 M NaCl)	10	6.08	20.03 ± 2.4		–
Affinity chromatography				–	
Eluted purified protein (25 mM imidazole)	2	5.01	37.86 ± 3.3		26
Cellulase from *A. niger* [a]	–	–	0.0 ± 1.1	65.7 ± 4.0	–
Empty vector pPICZαA [a]	–	–	4.24 ± 2.6	7.4 ± 2.7	–

XET Activity was assayed as Sulová et al. (1995) (Sulová et al., 1995) at pH 5.5. Values correspond to mean ± SE of four replicates.
XEH Activity was assayed as Arnal et al. (2017) (Arnal et al., 2017) at pH 5.5. Values correspond to mean ± SE of four replicates.
[a] Proteins extract used as control: cellulase from *A. niger* used as control for XEH activity; and the empty vector pPICZαA was used as XET and XEH basal yeast activities.

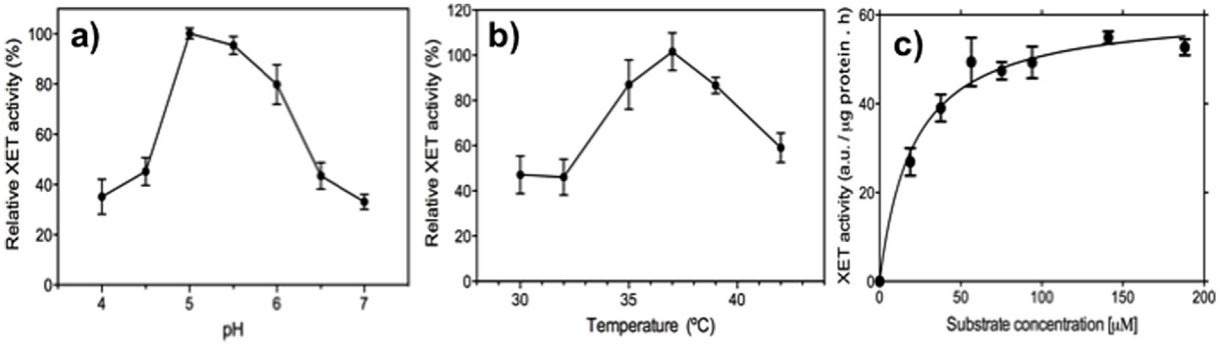

Fig. 1. Biochemical characterization of recombinant PrXTH1 protein. A) The pH dependence curve of XET activity of PrXTH1. B) The temperature dependence curve of XET activity of PrXTH1. C) Michaelis-Menten saturation curve of PrXTH1. Saturation curve were prepared with XGO. In the graphs bars indicate SE of four replicates.

Table 2
Kinetic parameters of purified PrXTH1 protein.

	K_M [a] (μM)	V_{max} [a] (a.u. μg^{-1} h^{-1})	k_{cat} (S^{-1})	k_{cat} * K_M^{-1} (S^{-1} μM^{-1})
PrXTH1	20.9 ± 2.7	61.3 ± 1.8	1.02 ± 0.03	0.049

XET activity was determined as Sulová et al. (1995)[26] with tamarind xyloglucan as donor substrate and XGO as acceptor substrate.
[a] Values were rounded to the first decimal point.

Table 3
Affinity energy of three different octasaccharides as putative ligands of PrXTH1 protein model by docking simulations using autodock vina.

Substrates	Affinity energy (kcal mol−1)
XLFGXLFG	−11,1
XXXGXXXG	−10,7
XXFGXXFG	−10,0
cellodextrin 8-mer	−6,9

and Braam, 1998; Rose et al., 2002; Fry, 2004; Johansson et al., 2004; Cosgrove, 2005; Minic and Jouanin, 2006). These enzymes belong to the glycosyl hydrolase family 16 (GH16) superfamily, which are encoded by a multigene family with 33 members in Arabidopsis (Yokoyama and Nishitani, 2001), 29 in rice (Yokoyama et al., 2004), 41 in poplar (Geisler-Lee et al., 2006), and 26 in *Fragaria vesca* (Opazo et al., 2017). The first eukaryotic 3D crystallographic XTH structure was PttXET16A from *Populus tremula* × *tremuloides* showing XET activity (Johansson et al., 2004). Its structural protein model has provided evidence for the mode of action of XTH proteins, and the relative importance of the loop between β-sheets 8 and 9 for hydrolase activity has been described (Baumann et al., 2007).

Recently, the model structure of the PrXTH1 was reported, displaying a β-sandwich structure characteristic of the XTH protein family, with the catalytic residues in the middle of the protein structure, composed of residues Glu79, Asp81, and Glu83 (Valenzuela et al., 2014). Additionally, Valenzuela et al. (2014) (Valenzuela et al., 2014) showed that the recombinant PrXTH1 purified protein has only transglycosylase (XET) activity. However, the kinetic properties or the interaction mode of the protein with its putative ligands has not yet been described.

Despite the knowledge generated in the past few years, there is still a limited understanding of the molecular mechanisms involved in cell wall remodeling. How does XTH protein interacts with different XG polymers at molecular level? and a better comprehension of cell wall metabolism during the inclination response are the main aim of this work. The characterization the PrXTH1 enzyme, structurally and biochemically can give clue on these aspects. A combination of bioinformatics (molecular docking and molecular dynamics simulations) and biochemical strategies were employed.

2. Methods

2.1. PrXTH1 protein production

The cloning of *PrXTH1* was previously reported by Valenzuela et al. (2014) (Valenzuela et al., 2014). The transformed *E.coli* was used for the production of recombinant PrXTH1 protein, which was carried out according to the method employed by Mendez-Yañez et al. (2017) (Mendez-Yañez et al., 2017). Briefly, the gene was expressed in *P. pastoris* and the production of protein was induces by methanol. The PrXTH1 protein was purified in two steps. First, by using a cation exchange chromatography (CMC, carboxymethyl cellulose resin, Sigma) in 50 mM sodium phosphate buffer (pH 6.0), and elution with 0.5 M NaCl; then, desalting through PD-10 columns (Sephadex™ G-25

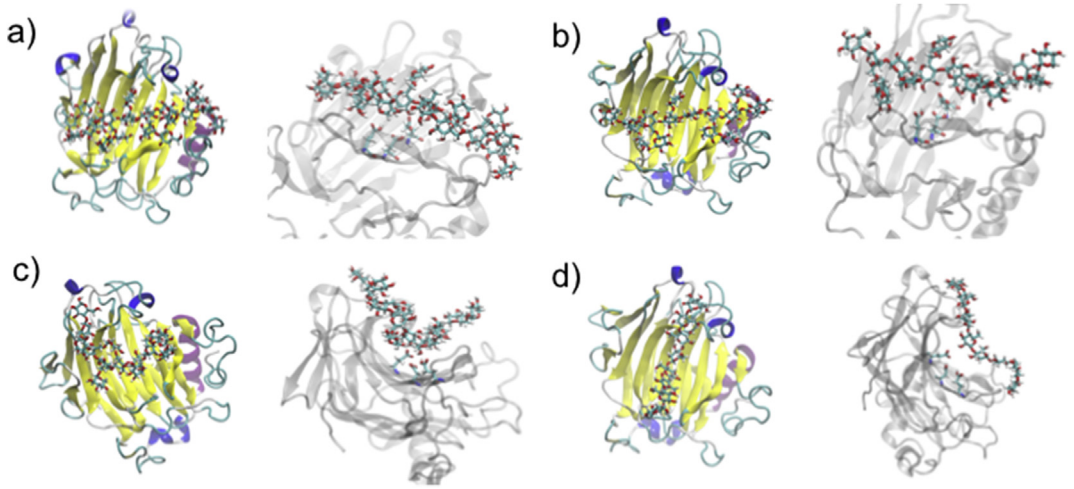

Fig. 2. Protein-ligand interaction of the PrXTH1 with hemicellulose octasaccharides and cellulose octasaccharide. A general view of the interaction of the protein and the corresponding ligand. In A) PrXTH1 with XLFGXLFG, B) PrXTH1 with XXXGXXXG, C) PrXTH1 with XXFGXXFG, and D) PrXTH1 with cellulose octasaccharide.

Medium) to remove salt and remaining CMC. The second step considers the use of an affinity chromatography (Talon Metal Affinity column, BD Biosciences) in the presence of 50 mM sodium phosphate buffer (equilibrium buffer at pH 7.4, washing buffer at pH 6.8), and finally protein was eluted with 0.025 M imidazole (pH 6.0). Protein concentration was determined according to Bradford method using bovine serum albumin as standard (Bradford, 1976). FcXTH1 protein expressed in yeasts was used as positive control, and the protein was purified using the same protocol (Mendez-Yañez et al., 2017).

2.2. Colorimetric XET assay

Enzyme activity was assayed by the colorimetric method described previously (Bradford, 1976), which is based on the overall XG-degrading activity (XDA) in the presence (XDA_{OS}) or absence (XDA_{O}) of XG oligosaccharides (XGOs). The XDA_{O} activity was measured in a reaction mixture of 200 µL total volume consisting of 0.2 mg tamarind xyloglucan (Megazyme) in 200 mM sodium acetate buffer (pH 5.5). XDA_{OS} was measured in the presence of 0.10 mg mL^{-1} XGOs (heptasaccharide X_3Glc_4, molecular weight 1062.9 g mol^{-1}, Megazyme). The reaction was initiated by the addition of 50 µg protein extract. The mixture was incubated during 2 h at 37 °C with gentle shaking. Aliquots (30 µL) were removed at the end of the incubation period. To each aliquot, 300 µL of 20% (w/v) Na_2SO_4 and 30 µL of I_2–KI solution (0.5% I_2 + 1% KI) were added, and after 30 min in the dark at room temperature changes in the absorbance at 620 nm were determined in an Epoch 2 Microplate Spectrophotometer (BioTek). The XG-transglycosylating (XET) activity was expressed as arbitrary units (a.u.) ug $protein^{-1}$ h^{-1} as described by Sulová et al. (1995) (Sulová et al., 1995). In our assay conditions, the reaction rate remains constant during the first 4 h of incubation, and therefore incubation periods of 2 h were adopted. Determinations were performed in four replicates and values correspond to means ± SE. Additionally, PrXTH1 inactivated enzyme by temperature (100 °C by 10 min) was used as negative control.

2.3. XEH activity assay

A sensitive reducing sugar assay was recently implemented to determine XTH activity (Arnal et al., 2017). The increment of the reducing sugars by BCA was followed through changes in absorbance at 562 nm determined in an Epoch 2 microplate spectrophotometer. Glucose was used as standard (0–50 µM). All measurements were performed in four replicates. PrXTH1 inactivated enzyme (by temperature, 100 °C by 10 min) was used as negative control.

2.4. pH profile and optimal temperature

To determine optimum assay conditions, pH was modified from 4 to 7, and the temperature ranged from 30 to 42 °C according to Mendez-Yañez et al. (2017) (Mendez-Yañez et al., 2017). XET activity was expressed in relative terms as % of the highest activity.

2.5. Kinetic parameters: K_M, V_{max} and k_{cat}

To determine kinetic parameters Michaelis − Menten saturation curves were built using XGOs as substrate (from 0.0 to 0.20 mg mL^{-1}) under standard assay conditions. Kinetic parameters were calculated from nonlinear least-squares data fitting (NLSF) in GraphPad Prism 6, using a Hanes–Woolf plot. Determinations were performed in quadruplicates and expressed as mean ± SE.

2.6. Protein-ligand interactions

Docking studies were performed to predict the putative binding between the PrXTH1 protein model previously described by Valenzuela et al. (2014) (Valenzuela et al., 2014) and different ligands: three hemicellulose octasaccharides (XXXGXXXG, XXFGXXFG, and XLFGXLFG) and one cellodextrin 8-mer that resembles a water-soluble cellulose molecule employed as negative control. The four ligands were built using GlyCAM-Web software (http://glycam.ccrc.uga.edu/), and ParamChem (Vanommeslaeghe et al., 1992) was used to provide and check the force field parameters required for the ligands. Autodock Vina v1 program (http://vina.scripps.edu/) (Trott and Olson, 2010) was used for the analysis.

Molecular Dynamics Simulation (MDS) of each substrate inside the active site of PrXTH1 was performed using NAnoscale Molecular Dynamics (NAMD) 2.12 (Phillips et al., 2005) with Chemistry at HARvard Macromolecular Mechanics (CHARMM) version 27 (MacKerell et al., 1992) force field for the protein and CHARMM version 36 (Guvench et al., 2009) for the carbohydrates, along with the TIP3P model for water (Jorgensen et al., 1983). The initial coordinates for MDS calculations were taken from the docking experiments. All simulations were performed during 50 ns according to the method employed by Gaete-Eastman et al. (2015) (Gaete-Eastman et al., 2015). During MDS, motion equations were integrated with a 2 fs time step in the canonical ensemble (NVT), with constant and pre-defined value of

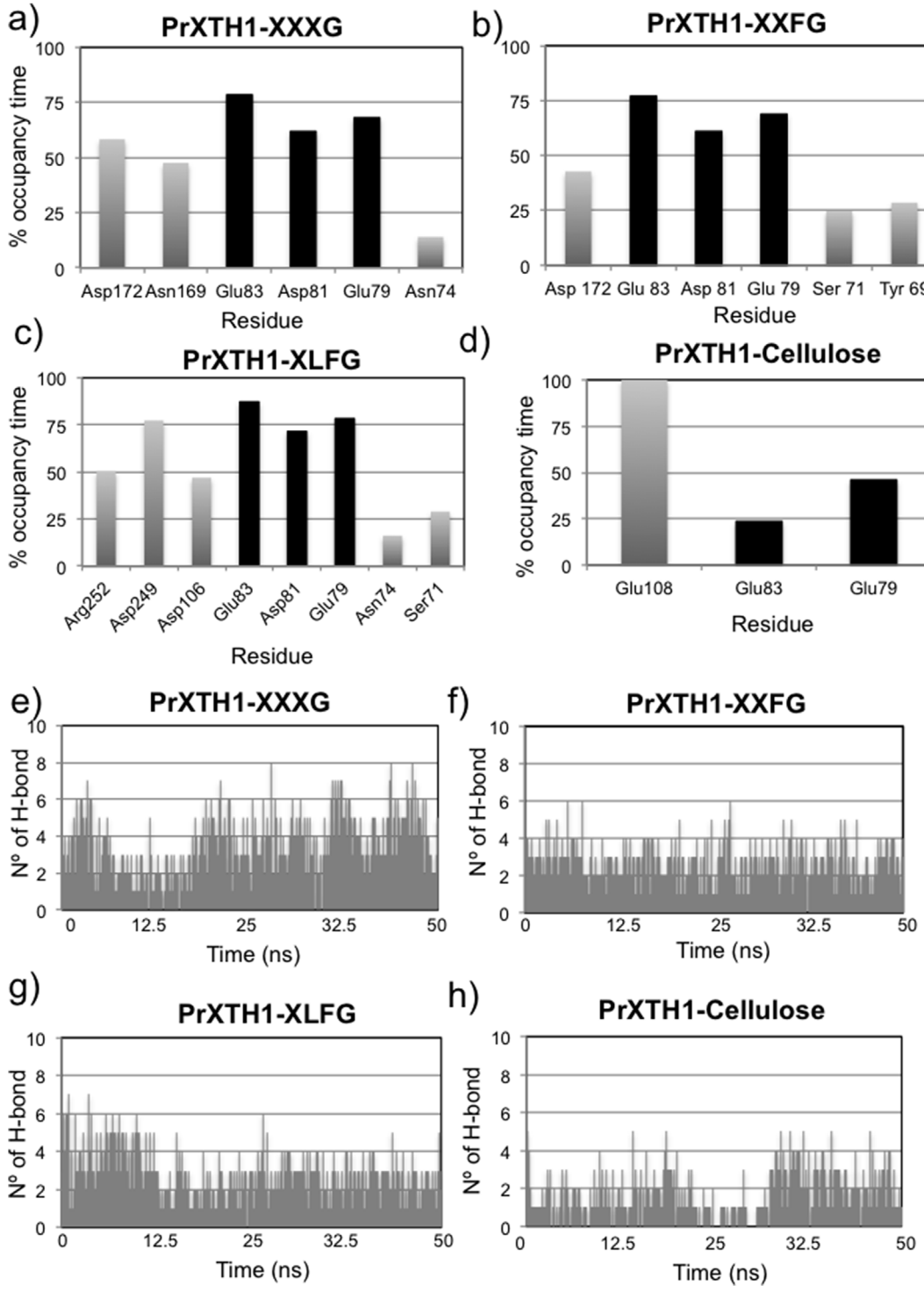

Fig. 3. MDS analysis of the PrXTH1 with the three hemicelluloses and cellulose as ligand. In A) to D) a graph indicating the percentage of time that a hydrogen bond between particular residue and the ligand is established during the MDS; the catalytic residues are shown in black, only values greater or equal of 15% frequency are shown in the graph. In E) to H) The number of the hydrogen bonds established during MDS between the ligand and different amino acid residues located in the open groove of PrXTH1.

the number of molecules (N), box size or volume (V) and temperature (T). The data were collected every 10 ps. Two replicates were used for each system. MM-GBSA (MM, Molecular Mechanics; GB, Generalized Born; SA, Surface Area) method (Homeyer and Gohlke, 2012) was employed according to Valenzuela-Riffo et al. (2015) (Valenzuela-Riffo et al., 2015) to estimate the relative free binding energy of protein-ligand complexes. Visualization of protein-ligand complexes and MD trajectory analyses were carried out with Visual Molecular Dynamics (VMD) v1.9.1 software (Humphrey et al., 1996).

2.7. Electrostatic potential

Using the adaptive Poisson–Boltzmann solver (APBS) (Baker et al., 2001) the electrostatic surfaces of PrXTH1 in complex with each of the four ligands was analyzed. A potential scale from −5 to +5 KT/e was employed in order to use the APBS software within VMD software

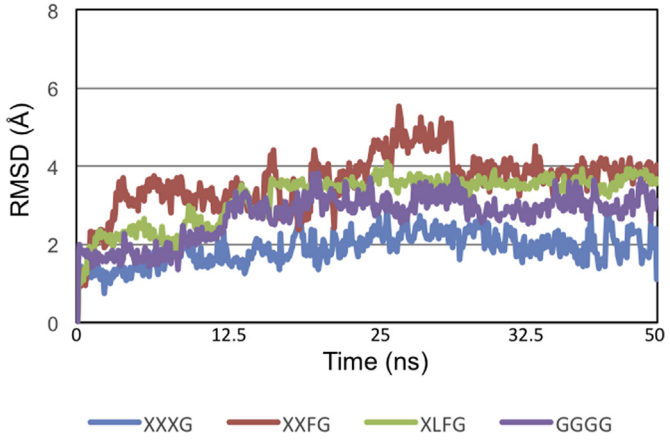

Fig. 4. RMSD values for each system evaluated during the MDS. The RMSD of the all atoms that form each protein-ligand complex.

(Humphrey et al., 1996).

3. Results and discussion

3.1. Characterization of PrXTH1 recombinant protein

P. pastoris yeast strains previously transformed with *PrXTH1* gene (Valenzuela et al., 2014) were induced with methanol for the expression of the recombinant protein. The authors purified the enzyme through an affinity chromatography (His-tag) and PrXTH1 protein displayed strict XET activity (Valenzuela et al., 2014). In here, the enzyme was further purified (13-fold purification) by the incorporation of an extra purification step: a cation exchange chromatography, and the analysis confirmed that PrXTH1 protein is effectively a strict XET enzyme (Table 1). This is coincident with the properties described for DkXTH1, DkXTH2 (Han et al., 2015), DkXTH6, DkXTH7 (Han et al., 2016), and DkXTH8 (Han et al., 2017) recombinant proteins from persimmon (*Diospyros kaki* L.) fruit, AtXTH15 from *Arabidopsis thaliana* (Shi et al., 2015), FcXTH1 from *Fragaria chiloensis* (Baumann et al., 2007), and PttXET16A from (*Populus tremula x tremuloides*) (Kallas et al., 2005). All of them showed significant XET activity without any detectable XEH activity.

As shown in Fig. 1a, the recombinant purified PrXTH1 protein exhibited a bell-shaped pH profile, with an optimum pH interval between pH 5.0 and 5.5. Furthermore, a rapid loss of XET activity was shown below pH 5; only 45% of activity remains at pH 4.5, and only 35% of activity at pH 4. This pH dependence is within the range reported for other XTHs previously described (Bradford, 1976; Han et al., 2015, 2016, 2017; Kallas et al., 2005). In addition, XET activity increases with temperature, and the optimum activity was obtained at 37 °C (Fig. 1b). Two different XTH have been described in term of optimal temperature. Some recombinant XTH proteins showed optimal temperature between 37°-40 °C (Bradford, 1976; Han et al., 2017). The dependence of the XET activity on the concentration of the added XGOs was analyzed (Fig. 1c). A saturation of the XET activity was observed at 140 μM (Fig. 1c).

3.2. Kinetic parameters of PrXTH1

The kinetic parameters (K_M and K_{cat}/K_M) of PrXTH1 enzyme were determined (Table 2). The K_M value determined was 20.9 μM, while the specificity (K_{cat}/K_M ratio) was 0.049 S^{-1} μM^{-1} (Table 2). The data obtained for PrXTH1 is similar to that of previously described XET enzymes (Bradford, 1976; Hrmova et al., 2009), however, PrXTH1 enzyme is apparently less specific than FcXTH1 or HvXET6 enzymes (K_{cat}/K_M ratios of 0.078 S^{-1} μM^{-1} and 0.087 S^{-1} μM^{-1}, respectively (Bradford, 1976; Hrmova et al., 2009)), but significantly more specific than HvXET5 enzyme (K_{cat}/K_M ratio of 0.0021 S^{-1} μM^{-1}) (Hrmova et al., 2009).

3.3. Substrate specificity of PrXTH1

A protein-ligand interaction study was carried out using the refined PrXTH1 model obtained previously by Valenzuela et al. (2014) (Valenzuela et al., 2014). Firstly, the protein-ligand conformation was evaluated using an automatic docking analysis. As shown in Table 3, favorable binding energies were obtained for the four ligands evaluated, nevertheless the interaction of PrXTH1 with the three hemicellulose octasaccharides was highly favored compared to the cellulose

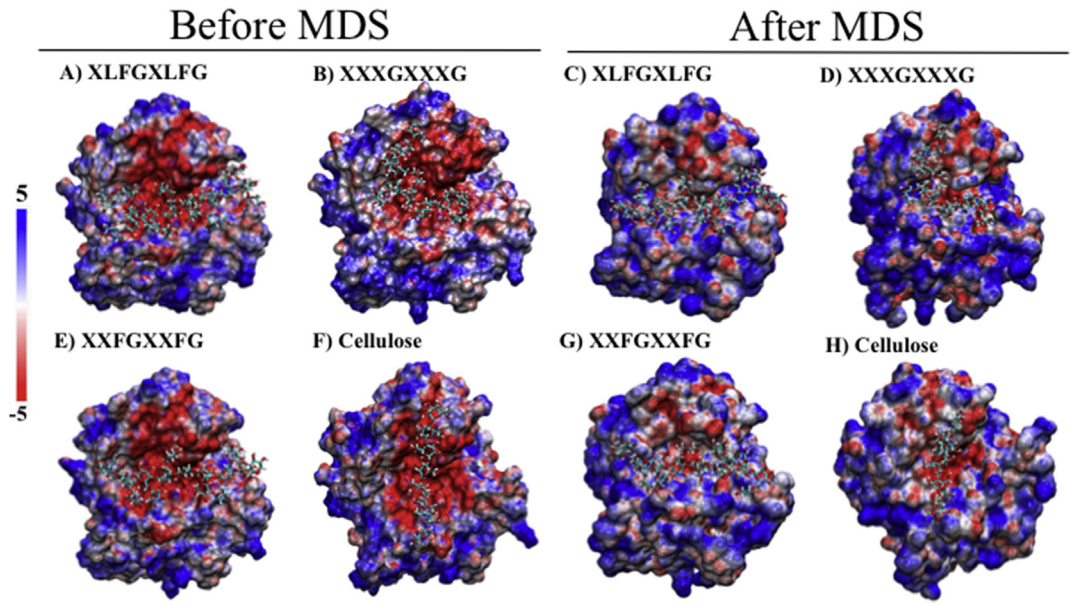

Fig. 5. Electrostatic potential of each protein-ligand complex before and after the molecular dynamics simulation. The electronegative zone is presented in red, the neutral zone in white and the electropositive zone in blue. (For interpretation of the references to color in this figure legend, the reader is referred to the Web version of this article.)

Table 4
MM-GBSA analyses for the interaction of PrXTH1 with different ligands.

Complexes	ΔH_{MM}^{vdW}(kcal mol^{-1})	ΔH_{MM}^{elec} (kcal mol^{-1})	$\Delta G_{sol-pol}$ (kcal mol-^{1})	$\Delta G_{sol-npol}$ (kcal mol^{-1})	ΔG_{bind} (kcal mol-^{1})
XLFGXLFG	−77.64	29.39	−1 x 10^{-4}	−10.57	−58.83 ± 0.8^{a}
XXXGXXXG	−76.60	32.13	−1 x 10^{-4}	−10.32	−54.78 ± 0.5^{b}
XXFGXXFG	−68.25	34.70	−1 x 10^{-3}	−8.78	−42.34 ± 0.6^{c}
cellodextrin 8-mer	−48.31	18.64	−1 x 10^{-4}	−5.76	−35.26 ± 0.3^{d}

ΔH_{MM}^{vdW}, van der Waals contributions; ΔH_{MM}^{elec}, electrostatic contribution; $\Delta G_{sol-pol}$, $\Delta G_{sol-npol}$, contribution of solvation; ΔG_{bind}, total binding energy.
Different superscripted letters indicate significant differences in each protein with the different ligands. (Tukey HSD test, P = 0.05).

octasaccharide (cellodextrin 8-mer) (Table 3). Fig. 2 displays the orientation of the ligands obtained from the different MD simulation analyses. In general, it can be observed that the different hemicellulose octasaccharides are positioned along the open groove of the protein, in contrast to cellulose that showed perpendicular orientation (Fig. 2). One of the main differences observed among the different protein-ligand complexes was the type and number of residues within the open groove that interact with each ligand. For example, the three hemicellulose ligands interact with the three catalytic residues (Glu79, Asp81 and Glu83) with occupancies over 60% during the MD trajectory (Fig. 3a, b, and 3c, black bars), while cellulose interacts with only two of the catalytic residues if we consider 20% of occupancy time as threshold (23% and 46% for Glu83 and Glu79, respectively) (Fig. 3d, black bars). The other catalytic residue (Asp81) does not interact with cellulose (occupancy time of 2.6%, data not shown). On the other hand, important differences were found in the number of hydrogen bonds formed between the different ligands and PrXTH1 model (Fig. 3e–h). In the case of PrXTH1 with XXXGXXXG, XLFGXLFG and XXFGXXFG as ligands more than three H-bonds were established during MD simulations (Fig. 3e–g), while only two H-bonds were established between PrXTH1 protein and cellodextrin (Fig. 3h). This trend is similar to a previous report (Mendez-Yañez et al., 2017) (Bradford, 1976) where a difference between the number of H-bonds generated between FcXTH1 and different ligands of XG type and cellulose was shown. Interestingly, Davies et al. (1997) (Davies et al., 1997) described two important sub-sites near to the active site of glycosyl hydrolase enzymes. These two sub-sites were named as positive or negative according to their position respect to the active site. Additionally, Mark et al. (2009) (Mark et al., 2009) showed for PttXET16-34 enzyme that residues from loops 2 and 3 were located either sides of the positive sub-sites (glycosyl acceptor-binding). When the interaction of PrXTH1 with hemicelluloses and cellulose as ligands were compared, a lower number of residues interact with cellulose in a stable manner (only 3 residues display more than 15% occupancy during MD simulation) than with hemicelluloses (Fig. 3a–d, grey bars). Finally, RMSD values for each system investigated are shown in Fig. 4. RMSD values were tested to check the convergence of the calculations and MD trajectory. RMSD values remained around 3–4 Å for XXFG, XLFG and cellulose systems, while PrXTH1-XXXG complex showed a RMSD value around 2 Å, demonstrating the conformational stability of the different protein-ligand structures (Fig. 4).

3.4. Electrostatic potential of PrXTH1

The electrostatic potential on the surface of PrXTH1 protein before and after the MD simulation was analyzed to further explain the differences in protein-ligand interaction between the protein and different ligands (Fig. 5). Interestingly, the four systems are mainly electronegative in the open groove region before MD simulation (Fig. 5), whereas after MD simulations, the open groove of PrXTH1 changes to electropositive form after the interaction with the three hemicellulose ligands (XXXG, XXFG and XLFG) (Fig. 5). However, it remains electronegative in the PrXTH1-cellulose complex (Fig. 5). This could explain in essence why the ligand is oriented differently on this complex respect to the other three ligands (Fig. 2).

3.5. Free binding energy estimated by MM-GBSA

To obtain more reliable estimates of free binding energy, MM-GBSA calculations for each protein-ligand complex were performed (Table 4). The analysis confirmed docking experiments as the affinity for cellodextrin is considerably lower than for the three hemicelluloses tested. There is a major contribution of van der Waals forces in the stability of the hemicelluloses complexes. The total binding energy indicates that the complex between PrXTH1 and XLFGXLFG is the most stable, followed by XXXGXXXG (Table 4). These results may be compared to those published for other XTHs. XET activity from AtXTH15 has better preference for XXXG as substrate than other XGOs (Shi et al., 2015), although the study in AtXTH15 was performed *in vitro*, these results are like the *in silico* data reported for FcXTH1 (Bradford, 1976). Albeit, a different ligand was determined for PrXTH1 because the higher ΔG_{bind} was with XLFGXLFG (Table 4). Additionally, when PrXTH1 and FcXTH1 ligand-complexes were compared, dramatic differences among the systems were determined for the same ligand. For example, in the case of XXXGXXXG as ligand, FcXTH1 binding energy was -95.3 kcal mol^{-1} (Bradford, 1976) compared to -42.3 kcal mol^{-1} for PrXTH1 (Table 4). On the other hand, the contribution of solvation ($\Delta G_{sol-pol} + \Delta G_{sol-npol}$) in MM-GBSA analysis of PrXTH1 did not show dramatic differences among the systems and did not affect the final ranking of affinities of the complexes (Table 4).

4. Conclusions

In conclusion, PrXTH1 recombinant enzyme has an optimal pH value between 5 and 5.5. PrXTH1 displays strict XET activity, which confirm previous studies. XET activity was saturated at 140 μM of XGOs concentrations (Fig. 1c). Additionally, our studies using the PrXTH1 structural model showed a better binding interactions with xyloglucans than cellulose, and in term of the different xyloglucan evaluated by MM-GBSA, the best ligand was the xyloglucan XLFGXLFG (Table 4). Even if it is necessary to complement how certain is this prediction, the current approximation to describe XTH enzyme from radiata pine is reported for the first time. Overall, the data provided allow us to propose that PrXTH1 activity plays an important role in response to inclination in radiata pine, suggesting an active participation in the reorganization and remodeling of the hemicellulose fraction at the cell wall.

Author contributions

DB, LM-Q, MAM-L and RH designed and performed the biochemical experiment. CC, LM-Q and RH designed and developed the structural bioinformatic analysis. LM-Q, RH and MAM-L wrote the manuscript.

Competing financial interests

The authors declare no competing financial interests.

Acknowledgments

This research was supported by FONDECYT #1150964 and

CONICYT PAI/Academia #79140027 projects. C.C. thanks CONICYT, Chile for his doctoral fellowship.

References

Arnal, G., Attia, M.A., Asohan, J., Brumer, H., 2017. A low-volume, parallel copper-bicinchoninic acid (BCA) assay for glycoside hydrolases. Methods Mol. Biol. 1588, 3–14. https://doi.org/10.1007/978-1-4939-6899-2.

Baker, N.A., Sept, D., Joseph, S., Holst, M.J., McCammon, J.A., 2001. Electrostatics of nanosystems: application to microtubules and the ribosome. Proc. Natl. Acad. Sci. U.S.A. 98, 10037–10041.

Baumann, M.J., Eklöf, J.M., Michel, G., Kallas, A.M., Teeri, T.T., Czjzek, M., Brumer, H., 2007. Structural evidence for the evolution of xyloglucanase activity from xyloglucan endo-transglycosylases: biological implications for cell wall metabolism. Plant Cell 19, 1947–1963.

Bradford, M.M., 1976. A rapid and sensitive method for the quantification of microgram quantities of protein utilizing the principle of protein dye binding. Anal. Biochem. 72, 248–254.

Campbell, P., Braam, J., 1998. Co- and/or post-translational modifications are critical for TCH4 XET activity. Plant J. 15, 553–561.

Carpita, N., McCann, M., The cell wall, Buchanan, B., Gruissem, W., Jones, R., Buchanan, B., Gruissem, W., 2000. In: Jones, R. (Ed.), Biochemistry and Molecular Biology of Plants. American Society of Plant Physiologists, Rockwell, MD, pp. 52–108.

Cosgrove, D.J., 2005. Growth of the plant cell wall. Nat. Rev. Mol. Cell Biol. 6, 850–861.

Davies, G.J., Wilson, K.S., Henrissat, B., 1997. Nomenclature for sugar-binding subsites in glycosyl hydrolases. Biochem. J. 321, 557–559.

Fry, S.C., 2004. Primary cell wall metabolism: tracking the careers of wall polymers in living plant cells. New Phytol. 161, 641–675.

Fry, S.C., York, W.S., Albersheim, P., Darvill, A., Hayashi, T., Joseleau, J.P., Kato, Y., Pérez Lorences, E., Maclachlan, G.A., McNeil, M., Mort, A.J., Grant, J.S., Hanns, R., Seitz, U., Selvendran, R.R., Voragen, A.G.J., White, A.R., 1993. An unambiguous nomenclature for xyloglucan-derived oligosaccharides. Physiol. Plantarum 89, 1–3.

Gaete-Eastman, C., Morales-Quintana, L., Herrera, R., Moya-León, M.A., 2015. *In silico* analysis of the structure and binding site features of expansin protein from mountain papaya fruit (VpEXP2), through molecular modelling, docking and dynamics simulation studies. J. Mol. Model. 21, 115. https://doi.org/10.1007/s00894-015-2656-7.

Geisler-Lee, J., Geisler, M., Coutinho, P.M., Segerman, B., Nishikubo, N., Takahashi, J., Aspeborg, H., Djerbi, S., Master, E., Andersson-Gunnera, S., Sundberg, B., Karpinski, S., Teeri, T.T., Kleczkowski, L.A., Henrissat, B., Mellerowicz, E.J., 2006. Poplar carbohydrate-active enzymes. Gene identification and expression analyses. Plant Physiol. 140, 946–962.

Gomez, R., Gonzalez, J., Herrera, R., Ramos, P., 2018. MYB Transcription Factors and a Putative Flavonoid Transporter ABCC-Like are Differentially Expressed in Radiata Pine Seedlings Exposed to Inclination. J. Plant Growth Regul. 37, 64–75. https://doi.org/10.1007/s00344-017-9707-5.

Guvench, O., Hatcher, E.R., Venable, R.M., Pastor, R.W., MacKerell, A.D., 2009. CHARMM Additive all-atom force field for glycosidic linkages between hexopyranoses. J. Chem. Theor. Comput. 5, 2353–2370.

Han, Y., Zhu, Q., Zhang, Z., Meng, K., Hou, Y., Ban, Q., Suo, J., Rao, J., 2015. Analysis of xyloglucan endotransglycosylase/hydrolase (XTH) genes and diverse roles of isoenzymes during persimmon fruit development and postharvest softening. PLoS One 10, 4. https://doi.org/10.1371/journal.pone.0123668e0123668.

Han, Y., Ban, Q., Hou, Y., Meng, K., Suo, J., Rao, J., 2016. Isolation and characterization of two Persimmon xyloglucan endotransglycosylase/hydrolase (XTH) genes that have diverget functions in cell wall modification and fruit postharvest softening. Front. Plant Sci. 7, 624. https://doi.org/10.3389/fpls.2016.00624.

Han, Y., Ban, Q., Li, H., Hou, Y., Jin, M., Han, S., Rao, J., 2017. DkXTH8, a novel xyloglucan endotransglucosylase/hydrolase in persimmon, alters cell wall structure and promotes leaf senescence and fruit postharvest softening. Sci. Rep. 6, 39155. https://doi.org/10.1038/srep39155.

Hoffman, M., Jia, Z., Pena, M.J., Cash, M., Harper, A., Blackburn, A.R., Darvill, A., York, W.S., 2005. Structural analysis of xyloglucans in the primary cell walls of plants in the subclass Asteridae. Carbohydr. Res. 340, 1826–1840.

Homeyer, N., Gohlke, H., 2012. Free energy calculations by the Molecular Mechanics Poisson-Boltzmann surface area method. Mol. Inf. 31, 114–122.

Hrmova, M., Farkas, V., Harvey, A.J., Lahnstein, J., Wischmann, B., Kaewthai, N., Ezcurra, I., Teeri, T.T., Fincher, G.B., 2009. Substrate specificity and catalytic mechanism of a xyloglucan xyloglucosyl transferase HvXET6 from barley (*Hordeum vulgare* L.). FEBS J. 276, 437–456.

Hsieh, Y.S., Harris, P.J., 2009. Xyloglucans of monocotyledons have diverse structures. Mol. Plant 2, 943–965.

Humphrey, W., Dalke, A., Schulten, K., 1996. VMD Visual molecular dynamics. J. Mol. Graph. 14, 33–38. https://doi.org/10.1016/0263-7855(96)00018-5.

Johansson, P., Brumer, H., Baumann, M.J., Kallas, A.M., Henriksson, H., Denman, S.E., Teeri, T.T., Jones, T.A., 2004. Crystal structures of a poplar xyloglucan endotransglycosylase reveal details of transglycosylation acceptor binding. Plant Cell 16, 874–886.

Jorgensen, W.L., Chandresekhar, J., Madura, J.D., 1983. Comparison of simple potential functions for simulating liquid water. J. Chem. Phys. 79, 926–935.

Kallas, A.M., Piens, K., Denman, S.E., Henriksson, H., Faldt, J., Johansson, P., Brumer, H., Teeri, T.T., 2005. Enzymatic properties of native and deglycosylated hybrid aspen (*Populus tremula x tremuloides*) xyloglucan endotransglycosylase 16A expressed in *Pichia pastoris*. Biochem. J. 390, 105–113.

MacKerell Jr., A.D., Bashford, D., Bellott, M., Dunbrack Jr., R.L., Evanseck, J., Field, M., Fischer, J.S., Gao, J., Guo, H., Ha, S., Joseph, D., Kuchnir, L., Kuczera, K., Lau, C., Mattos, F.T.K., Michnick, S., Ngo, T., Nguyen, D.T., Prodhom, B., Roux, B., Schlenkrich, M., Smith, J., Stote, R., Straub, J., Watanabe, M., Wiorkiewicz-Kuczera, J., Yin, D., Karplus, M., 1992. Self-consistent parametrization of biomolecules for molecular modeling and condensed phase simulations. FASEB J. 6, A143.

Mark, P., Baumann, J.M., Eklöf, J.M., Gullfot, F., Michel, G., Kallas, A.M., Teeri, T.T., Brumer, H., Czjzek, M., 2009. Analysis of nasturtium TmNXG1 complexes by crystallography and molecular dynamics provides detailed insight into substrate recognition by family GH16 xyloglucan endo-transglycosylases and endohydrolases. Proteins 75, 820–836.

Mateluna, P., Valenzuela, F., Morales-Quintana, L., Herrera, R., Ramos, P., 2017. Transcriptional and computational study of expansins differentially expressed in response to inclination in radiata pine. Plant Physiol. Biochem. 115, 12–24.

Mendez-Yañez, A., Beltrán, D., Campano-Romero, C., Molinett, S., Herrera, R., Moya-León, M.A., Morales-Quintana, L., 2017. Glycosylation is important for FcXTH1 activity as judged by its structural and biochemical characterization. Plant Physiol. Biochem. 119, 200–210.

Minic, Z., Jouanin, L., 2006. Plant glycoside hydrolases involved in cell wall polysaccharide degradation. Plant Physiol. Biochem. 44, 435–449.

Muday, G.K., 2001. Auxins and tropisms. J. Plant Growth Regul. 20, 226–243.

Opazo, C., Lizana, R., Stappung, Y., Davis, T.M., Herrera, R., Moya-León, M.A., 2017. XTHs from *Fragaria vesca*: genomic structure and transcriptomic analysis in ripening fruit and other tissues. BMC Genomics 18, 852. https://doi.org/10.1186/s12864-017-4255-8.

Peña, M.J., Darvill, A.G., Eberhard, S., York, W.S., O'Neill, M.A., 2008. Moss and liverwort xyloglucans contain galacturonic acid and are structurally distinct from the xyloglucans synthesized by hornworts and vascular plants. Glycobiology 18, 891–904.

Phillips, J.C., Braun, R., Wang, W., Gumbart, J., Tajkhorshid, E., Villa, E., Chipot, C., Skeel, R.D., Kale, L., Schulten, K., 2005. Scalable molecular dynamics with NAMD. J. Comput. Chem. 26, 1781–1802. https://doi.org/10.1002/jcc.20289.

Ramos, P., Herrera, R., 2013. Anatomical changes of xylem cells in stem of *Pinus radiata* seedlings exposed to inclination and ethylene. Biol. Plant. 57, 525–530.

Ramos, P., Le Provost, G., Plomion, C., Gantz, C., Herrera, R., 2012. Transcriptional analysis of differential expressed genes in response to stem inclination in young seedlings of pine. Plant Biol. 14, 923–933.

Ramos, P., Guajardo, J., Moya-León, M.A., Herrera, R., 2016. A differential distribution of auxin and flavonols in radiata pine stem seedlings exposed to inclination. Tree Genet. Genomes 12, 42. https://doi.org/10.1007/s11295-016-1003-1.

Rose, J.K.C., Braam, J., Fry, S.C., Nishitani, K., 2002. The XTH family of enzymes involved in xyloglucan endotransglucosylation and endohydrolysis: current perspectives and a new unifying nomenclature. Plant Cell Physiol. 43, 1421–1435.

Shi, Y.Z., Zhu, X.F., Miller, J.G., Gregson, T., Zheng, S.J., Fry, S.C., 2015. Distinct catalytic capacities of two aluminium-repressed Arabidopsis thaliana xyloglucan endotransglucosylase/hydrolases, XTH15 and XTH31, heterologously produced in Pichia. Phytochemistry 112, 160–169.

Sulová, Z., Lednická, M., Farkâs, V., 1995. A colorimetric assay for xyloglucan endotransglycosylase from germinating seeds. Anal. Biochem. 229, 80–85.

Trott, O., Olson, A.J. AutoDockVina, 2010. improving the speed and accuracy of docking with a new scoring function, efficient optimization and multithreading. J. Comput. Chem. 31, 455–461. https://doi.org/10.1002/jcc.21334.

Tuomivaara, S.T., Yaoi, K., O'Neill, M.A., York, W.S., 2015. Generation and structural validation of a library of diverse xyloglucan-derived oligosaccharides, including an update on xyloglucan nomenclature. Carbohydr. Res. 402, 56–66.

Valenzuela, C., Ramos, P., Carrasco, C., Moya-León, M.A., Herrera, R., 2014. Cloning and characterization of a xyloglucan endo-transglycosylase/hydrolase gene expressed in response to inclination in radiata pine seedlings. Tree Genet. Genomes 10, 1305. https://doi.org/10.1007/s11295-014-0762-9.

Valenzuela-Riffo, F., Tapia, G., Parra-Palma, C., Morales-Quintana, L., 2015. Understanding the roles of Lys33 and Arg45 in the binding site stability of LjLTP10 an LTP related with drought stress in *Lotus japonicus*. J. Mol. Model. 21, 270. https://doi.org/10.1007/s00894-015-2807-x.

Vanommeslaeghe, K., Hatcher, E., Acharya, C., Kundu, S., Zhong, S., Shim, J., Darian, E., Guvench, O., Lopes, P., Vorobyov, I., Mackerell, A.D., 1992. CHARMM general force field: A force field for drug-like molecules compatible with the CHARMM all-atom additive biological force fields. J. Comput. Chem. 31, 671–690.

Yokoyama, R., Nishitani, K., 2001. Endoxyloglucan transferase is localized both in the cell plate and in the secretory pathway destined for the apoplast in tobacco cells. Plant Cell Physiol. 42, 292–300.

Yokoyama, R., Rose, J.K.C., Nishitani, K., 2004. A surprising diversity and abundance of xyloglucan endotransglucosylase/hydrolases in rice. Classification and expression analysis. Plant Physiol. 134, 1088–1099.